Heliyon 10 (2024) e32140

Contents lists available at ScienceDirect

Heliyon

journal homepage: www.cell.com/heliyon

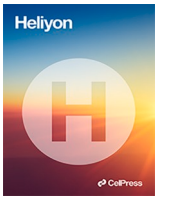

Research article

Nanomolar concentrations of the photodynamic compound TLD-1433 effectively inactivate numerous human pathogenic viruses

Kevin M. Coombs [a,b,*], Kathleen K.M. Glover [a,b], Raquel Russell [a,b,1], Pavel Kaspler [c], Mark Roufaiel [c], Drayson Graves [d], Peter Pelka [d], Darwyn Kobasa [e], Roger DuMoulin-White [c], Arkady Mandel [c]

[a] Department of Medical Microbiology and Infectious Diseases, University of Manitoba, Winnipeg, Manitoba, R3E 0J9, Canada
[b] Manitoba Centre for Proteomics and Systems Biology, University of Manitoba, Winnipeg, Manitoba, R3E 3P4, Canada
[c] Theralase® Technologies Inc., 41 Hollinger Road, Toronto, Ontario, M4B 3G4, Canada
[d] Department of Microbiology, University of Manitoba, Winnipeg, Manitoba, R3T 2N2, Canada
[e] Special Pathogens Program, National Microbiology Laboratory, Public Health Agency of Canada, Winnipeg, Manitoba, R3E 3R2, Canada

ARTICLE INFO

Keywords:
Antivirals
Lipid envelope
Photodynamic therapy
TLD-1433
Ruvidar™

ABSTRACT

The anti-viral properties of a small (≈1 kDa), novel Ru(II) photo dynamic compound (PDC), referred to as TLD-1433 (Ruvidar™), are presented. TLD-1433 had previously been demonstrated to exert strong anti-bacterial and anti-cancer properties. We evaluated the capacity of TLD-1433 to inactivate several human pathogenic viruses. TLD-1433 that was not photo-activated was capable of effectively inactivating 50 % of influenza H1N1 virus (ID_{50}) at a concentration of 117 nM. After photo-activation, the ID_{50} was reduced to <10 nM. The dose of photo-activated TLD-1433 needed to reduce H1N1 infectivity >99 % (ID_{99}) was approximately 170 nM. Similarly, the ID_{99} of photo-activated TLD-1433 was determined to range from about 20 to 120 nM for other tested enveloped viruses; specifically, a human coronavirus, herpes simplex virus, the poxvirus Vaccinia virus, and Zika virus. TLD-1433 also inactivated two tested non-enveloped viruses; specifically, adenovirus type 5 and mammalian orthoreovirus, but at considerably higher concentrations. Analyses of TLD-1433-treated membranes suggested that lipid peroxidation was a major contributor to enveloped virus inactivation. TLD-1433-mediated virus inactivation was temperature-dependent, with approximately 10-fold more efficient virucidal activity when viruses were treated at 37 °C than when treated at room temperature (~22 °C). The presence of fetal bovine serum and virus solution turbidity reduced TLD-1433-mediated virucidal efficiency. Immunoblots of TLD-1433-treated human coronavirus indicated the treated spike protein remained particle-associated.

* Corresponding author. Department of Medical Microbiology and Infectious Diseases, University of Manitoba, Winnipeg, Manitoba, R3E 0J9, Canada.

E-mail addresses: kevin.coombs@umanitoba.ca (K.M. Coombs), gloverk@myumanitoba.ca (K.K.M. Glover), russell2@myumanitoba.ca (R. Russell), pkaspler@theralase.com (P. Kaspler), mroufaiel@theralase.com (M. Roufaiel), gravesd@myumanitoba.ca (D. Graves), peter.pelka@umanitoba.ca (P. Pelka), darwyn.kobasa@phac-aspc.gc.ca (D. Kobasa), rwhite@theralase.com (R. DuMoulin-White), amandel@theralase.com (A. Mandel).

[1] Current address: Rapid Novor, Inc., 137 Glasgow St., Unit 450, Kitchener, Ontario N2G 4X8, Canada.

https://doi.org/10.1016/j.heliyon.2024.e32140
Received 8 January 2024; Received in revised form 28 May 2024; Accepted 29 May 2024
Available online 29 May 2024

1. Introduction

Infectious agents (*e.g.* bacteria, fungi, parasites, and viruses) remain a major cause of morbidity and mortality and still account for more than 10,000,000 deaths annually (www.who.int/data/gho/data/themes/mortality-and-global-health-estimates/ghe-leading-causes-of-death). Several agents, such as SARS-CoV-2, responsible for the current COVID-19 pandemic, are either new or newly re-emerging [1,2]. Furthermore, it is suggested that with rising antibiotic resistance, infections by resistant bacteria may account for significantly higher death rates within a few decades [3].

Abbreviations

Ad5	Adenovirus, strain 5
CoV	Coronavirus
CPE	cytopathic effect
DMEM	Dulbecco's minimal essential medium
EMEM	Eagle's minimal essential medium
JMEM	Joklik's modified essential medium
HPF	High power field
HSV-1	Herpes simplex virus, type 1
IAV	Influenza virus
MOI	multiplicity of infection
MRV	Mammalian (ortho)reovirus
PDC	Photodynamic compound
PDT	Photodynamic therapy
PEG	Polyethylene glycol
ROS	Reactive oxygen species
VACV	Vaccinia virus
ZIKV	Zika virus

There are several accepted strategies to combat infectious agents, including vaccines and anti-microbials. Vaccines are useful when administered prior to infection, whereas antibiotics and anti-virals are most useful after infection or before immunity to a vaccine has time to develop. Primary disadvantages of vaccines are that knowledge of the agent is required in advance and substantial time is needed to produce relevant vaccines. This strategy has been the mainstay for annual influenza vaccine programs, but sometimes the vaccine does not match the eventual circulating virus strain [4,5]. A growing number of anti-viral agents have been developed and some are effective against numerous viruses. However, because viruses replicate and many lack genome proof-reading capabilities, resistance to the anti-viral agent may rapidly develop [6–8].

Photodynamic therapy (PDT) is a potential strategy that has been demonstrated effective against various cancers [9–13], bacterial pathogens [14,15] and viruses [16–20]. PDT is based upon the use of a photodynamic compound (PDC) that is administered to the pathogen in question, then activated by exposure to a particular wavelength(s) of light to produce reactive oxygen species (ROS) which effects microbial or cancer killing [15,18]. Originally found to kill paramecia, a variety of different PDCs have been developed and tested over the years, with 3rd and 4th generation PDCs now under investigation (reviewed in Refs. [12,21]).

TLD-1433 (Ruvidar™) is a ruthenium(II)-based 4th generation PDC, that has been developed and studied for more than a decade by Theralase®. It is a complex with the formula $[Ru(II)(4,4'\text{-dmb})_2(IP\text{-}3T)]Cl_2$, where 4,4′-dmb = 4,4′-dimethyl-2,2′-bipyridine; IP = imidazo [4,5], [1,10]phenanthroline; and 3T = α-terthienyl (an oligomer consisting of three tyophenes) (Fig. 1a). Based on interim

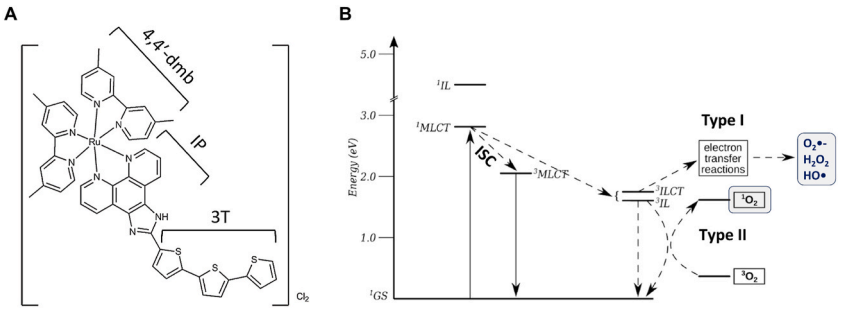

Fig. 1. A, Structural formula of Ruvidar™ (TLD-1433) and B, Energy transfer and relaxation (Jablonski diagram) in TLD-1433 upon excitation by visible light. Generation of $^1O_2$ Type I photoreaction (energy transfer) and other reactive oxygen species (ROS) including free radicals as Type II photoreaction (electron transfer) is shown as the end result of TLD-1433 excitation. Adapted and modified from Ref. [24].

clinical data, it has demonstrated high efficacy, strong duration of response and high safety in a Phase II clinical study focused on the treatment of patients diagnosed with high-grade, Bacillus Calmette-Guérin (BCG)-unresponsive, non-muscle invasive bladder cancer (NMIBC) carcinoma in-situ (CIS) (with or without resected T_a/T_1 papillary disease). This registration clinical study is intended to be the basis for initial regulatory approval of Ruvidar™ in Canada and in the US for this oncological condition [9,22]. TLD-1433 also is effective against Gram-negative *E. coli* [23], and various Gram-positive bacteria such as *S. aureus* and *MRSA* [14]. Arenas and colleagues demonstrated that TLD-1433 was effective in killing *S. aureus* and *MRSA* at dosages ~1000-fold lower than methylene blue [14]. Given its current usage and effectiveness against bacteria, we tested whether it also was effective against several human pathogenic viruses and discovered that nanomolar concentrations were effective in inactivating >99 % of numerous viruses. In addition, TLD-1433-mediated PDT did not appear to remove antigenic epitopes from a tested human coronavirus.

2. Materials & methods

2.1. Cells and viruses

Human lung A549 (ATCC #CCL-185) and monkey kidney Vero cells (ATCC #CCL-81) were cultured in DMEM supplemented with 1 × L-glutamine, 1 × non-essential amino acids, 1 × sodium pyruvate, and 10 % FBS (Gibco; Cat #10437028). MDCK cells (ATCC #CCL-34) were cultured in the same media but supplemented with 5 % FBS instead of 10 %. MRC-5 cells (ATCC #CCL-171) were cultured in ATCC EMEM (Cat #30–2003) supplemented with 10 % FBS. Mouse L929 cells were cultured in JMEM supplemented with 1 × L-glutamine and 7.5 % FBS. All cells were trypsinized and sub-cultured at 1:6–1:10 ratios 3 times a week.

Adenovirus type 5 (Ad5) was propagated and titrated in A549 cells. Coronavirus OC-43 was propagated and titrated in MRC-5 cells. Herpes simplex virus-1 (HSV-1), Vaccinia virus (VACV) strain WWR, and Zika virus (ZIKV) were propagated and titrated in Vero cells. Influenza A virus (IAV) strains A/PR/8/34(H1N1; PR8) and A/California/07/2009(H1N1; pdm09) were propagated and titrated in MDCK cells. Mammalian orthoreovirus (MRV), strain type 1 Lang (T1L) was propagated in murine L929 cells.

2.2. Preparation of high titer stock viruses

If required, OC-43 and IAV stocks were concentrated by centrifuging infected culture supernatants at 45,000×*g* for 2h in a Beckman JA-25.50 rotor and resuspended in small volumes of PBS. Ad5 and T1L were concentrated by harvesting infected cells, pelleting them and resuspending the infected cells in 1/30th the supernatant volume, followed by 3 freeze/thaw cycles.

To prepare high-titer HSV-1, Vero cells in 60 × 15-cm tissue culture dishes were infected with HSV-1 at a multiplicity of infection (MOI) of 0.001 plaque forming units (PFU)/cell and incubated at 37 °C for 3–4 days until cytopathic effect (CPE) was >90 %. Culture supernatants were clarified at 1200×*g* to remove cellular debris, and pooled virus precipitated by addition of NaCl by 0.5 M and 1/3 volume of 40 % PEG8000. After overnight precipitation at 5 °C with constant stirring, precipitated virus was pelleted at 2500×*g* for 60min, resuspended in 10 ml PBS, and banded in potassium tartrate/sucrose gradients (15/10 % - 30/25 %) at 80,000×*g* for 6h. The purified virus was aliquoted and frozen at −80 °C and had a measured titer of 5×10^{10} PFU/ml.

To prepare high-titer VACV, Vero cells in ten 15-cm tissue culture dishes were infected with VACV at an MOI of 0.01 PFU/cell and incubated at 37 °C for 3–4 days until CPE was >90 %. The supernatants were collected and virus pelleted at 15,000×*g* for 30min. Cells were harvested, washed 2 × with PBS and resuspended in 5 ml of 10 mM NaCl, 10 mM Tris, pH 7.2. The cells were swollen on ice for 30min and lysed with 10 strokes of a tight-fitting stainless steel Dounce homogenizer. Cell nuclei were removed by centrifugation at 500×*g* for 5min and the resulting milky white supernatant used to resuspend the pelleted supernatant virus, then made 10 % glycerol, aliquoted and frozen at −80 °C. This preparation had a measured titer of 3×10^9 PFU/ml.

2.3. Infectious virus enumeration

Viral titers were determined by plating serial 1:10 dilutions of various virus stocks or of treated virus. Briefly, Ad5 titers were determined by plaque assay on A549 cell monolayers in 12-well plates. 1:10 dilutions were overlaid with 0.6 % Agarose in 1 × DMEM supplemented with 3.75 % FBS and 1 × L-glutamine, 1 × non-essential amino acids, 1 × sodium pyruvate, and 20 mM $MgCl_2$, incubated at 37 °C for 5 days, and stained with 0.04 % neutral red. OC-43 titers were determined by immuno-focus assay as described [25]. Briefly, 50 μL aliquots of 1:10 dilutions were added to MRC-5 monolayers in 48-well plates. After 1h adsorption in a 33.5 °C incubator with periodic rocking, infected cells were overlaid with 1 % Avicel® in 1 × Medium 199 (M199) supplemented with 0.25 % BSA and 1 μg/ml trypsin. Overlaid cells were incubated at 33.5 °C for 38–40h, washed 1 × with PBS and fixed in PBS +3 % formaldehyde. After fixation for > 6h, cells were gently lysed with 0.1 % NP-40, blocked overnight in TBST + either 0.3 % BSA or 5 % skim milk, and probed with mouse α–OC–43 N protein antibody (Sigma-Aldrich Cat #MAB9013). Immune complexes were detected with an HRP-conjugated α-mouse 2° antibody and TrueBlue® peroxidase substrate. HSV-1 titers were determined by plaque assay on Vero cell monolayers. 1:10 dilutions were overlaid with 0.6 % Agarose in 1 × M199 supplemented with 3 % FBS and 1 × L-glutamine, incubated at 37 °C for 3 days, and stained with 0.04 % neutral red. IAV titers were determined by plaque assay on MDCK cell monolayers. 1:10 dilutions were overlaid with 0.8 % Avicel® in 1 × DMEM supplemented with 2.5 μg/ml trypsin. Overlaid cells were incubated at 33.5 °C for 3 days, washed 1 × with PBS and fixed in PBS +3 % formaldehyde. After fixation for > 6h, cells were stained with crystal violet. MRV T1L titers were determined by plaque assay on L929 cell monolayers. 1:10 dilutions were overlaid with 1 % Agar in 1 × M199 supplemented with 3 % FBS and 1 × L-glutamine, incubated at 37 °C for 6 days, and stained with 0.04 % neutral red. VACV titers were determined by plaque assay on Vero cell monolayers. 1:10 dilutions were overlaid with DMEM supplemented with 5 % FBS, 1 ×

non-essential amino acids, 1 × sodium pyruvate and 1 × L-glutamine, incubated at 37 °C for 3 days, cell monolayers fixed with 3 % formaldehyde and stained with 1 % crystal violet. Plates were washed and air dried. ZIKV titers were determined by plaque assay on Vero cell monolayers. 1:10 dilutions were overlaid with 0.6 % Agarose in 1 × M199 supplemented with 3 % FBS and 1 × L-glutamine, incubated at 37 °C for 4 days, and stained with 0.04 % neutral red.

2.4. Virus inactivation

The Theralase® PDC Ruvidar™ (TLD-1433) was freshly prepared for each experiment by dissolving a pinch of powder in sterile d.H_2O. TLD-1433 concentration was determined by measuring OD_{440} (100 μL of solution, and of dH_2O as blank, in individual wells in a 96-well plate) and using the empirically determined extinction coefficient of 1 OD_{440} = 183 μM. A variety of sub-stock solutions, representing 20 × concentrations of desired final concentrations, were made by sequential dilution into $d.H_2O$.

Aliquots of 122 μL of each chosen virus were placed into individual wells of 96-well plates and 6.4 μL of each 20 × TLD-1433 concentration added to achieve final TLD-1433 concentrations ranging from 0.1 nM–100 μM. Mixtures were divided into two replicate plates. Both plates were incubated in the dark at various temperatures for various periods of time. One of the replicate plates then was exposed to green light at a wavelength of 525 ± 25 nm and an energy density of 45 J/cm^2 for various periods of time. The light-treated and dark-treated samples were allowed to rest for 15 min and then residual virus infectivity determined by focus assay or plaque assay as described above.

2.5. CoV spike protein immunogenicity

Equivalent aliquots of OC-43 were treated with 0 or 250 nM of TLD-1433, incubated for 30 min at room temperature and exposed to light for 75 s. After resting an additional 15 min, virus structures were pelleted by centrifugation at 45,000×*g* for 90 min in a Beckman JA-25.50 rotor. The supernatants and pellets were separately collected. Pellets were resuspended in the original volume of PBS and electrophoresis sample buffer was added to each sample. Viral proteins were resolved in 10 % SDS-PAGE and transferred to nitrocellulose membranes, then blocked with 5 % skim milk and probed with mouse α–OC–43 S protein antibody (Abbexa Cat #ABX109271). Immune complexes were detected with a goat HRP-conjugated α-mouse 2° antibody (Cell Signaling Cat #7076) and visualized with an Alpha Innotech FluorChemQ MultiImage III machine.

2.6. Testing Ruvidar™-treated virus capacity to induce cytopathic effect

High-titer HSV-1 was diluted to a final concentration of $>1 \times 10^9$ PFU/ml with PBS and set up as five aliquots of 1.1 mL. TLD-1433 was added to final concentrations of 1.0 μM to two aliquots, to final concentrations of 3.16 μM to two aliquots, and to a final concentration of 10 μM to one aliquot. Each sample was then dispensed into 18 wells in 96-well plates (~66 μL per well) and incubated at 37 °C for 30 min. One of each TLD-1433 concentration-treated sample was irradiated with green light at a wavelength of 525 ± 25 nm and an energy density of 45 J/cm^2 for 75 s. The other two samples (treated with 1.0 and 3.16 μM TLD-1433) were irradiated for 150 s. After a 15 min rest period, each sample was collected and used to infect Vero cells in 10 cm dishes (effective limit of detection <1 PFU). In parallel, Vero cells in 6-well plates were infected with known concentrations of HSV-1 corresponding to 0 (6 samples), 1 PFU (6 samples), 2 PFU (6 samples), 4 PFU (2 samples), and 1 sample each of 10, 100, and 1000 PFU. Additional wells in 6-well plates were treated with HSV-1 that had been treated with 31.6 or 316 nM of TLD-1433. The cells were incubated for six days and monitored for CPE. On the 6th day, 1 ml of the 10 cm cultures were transferred to additional 10 cm dishes for the 2nd passage and 250 μL of each 6-well culture were transferred to additional 6-well plates of Vero cells. Cells were incubated and monitored for CPE for an additional 6 days and a 3rd passage set up after the 6th day, which was also monitored for CPE.

2.7. Singlet oxygen and hydroxyl radical measurements

Reactive oxygen species (ROS; $^1O_2$) were measured with 100 μM fluorescent SOGS reporter and hydroxyl radicals (*HO) were measured using 100 μM fluorescent HPF as described [26]. Briefly, SOGS or HPF were added to a solution of 3 μM Ruvidar™ in DMEM not supplemented with FBS in wells in a 96-well plate. The solutions then were exposed to 535 nm LED laser light (227 mW/cm^2) for defined time intervals, and generation of ROS by Ruvidar™ was measured for each timepoint: singlet oxygen signal (at 494 nm excitation and 525 nm emission for SOSG) and hydroxyl radical signal (at 490 nm excitation and 515 nm emission for HPF). During the ROS measurements, the signals in the presence of only indicator in medium but with no Ruvidar™ served as a non-specific reference and were subtracted from the overall signals generated by Ruvidar™ in the presence of indicator. The signals were read in duplicate for each experiment on a 96-well plate reader (SpectroMax, Molecular Devices, Sunnyvale, CA, U.S.A.) and the experiment was repeated 5 to 7 times depending on the time point of energy delivered.

2.8. Lipid peroxidation determination

Lipid peroxidation was determined in crude membranes extracted from A549 cells. The cells were grown in 75 cm^2 flasks, expanded overnight in 175 cm^2 flasks, washed with PBS, scraped off the flask and resuspended in 6 mL of fresh PBS. The cell suspension was centrifuged at 300×*g* for 5 min at 4 °C. The resulting pellet was resuspended in 5 mL of hypotonic buffer (20 mM HEPES, 10 mM KCl, 2 mM $MgCl_2$, 1 mM EDTA, 1 mM EGTA, pH = 7.4) and incubated on ice for 15 min. Following that, the cells were disrupted using a Sonic

Vibracell VC130 sonicator (Sonics & Materials Inc., Newtown, CT, USA) at 40 nm amplitude. The sonication cycle consisted of sonication for 10 s and rest on ice for 30 s; the complete sonication process consisted of six cycles. After sonication, a small aliquot of suspension was monitored by microscopy to ensure completeness of cell disruption. The resulting lysate was incubated on ice for 20 min and centrifuged at 800×*g* for 10 min at 4 °C. The supernatant was centrifuged at 5000×*g* for 5 min at room temperature, transferred to new tubes and centrifuged again at 16,000×*g* for 20 min at room temperature. The resulting crude membrane pellet was resuspended in 200 μL of TBS buffer (20 mM Tris, 150 mM NaCl, pH = 7.6) and frozen at −80 °C until further use.

To perform lipid peroxidation, the membrane suspension was incubated with 1 μM TLD-1433 (prepared from 1.6 mM stock made in d.H_2O) for 30 min at room temperature in 96-well plates, with 100 μL membrane aliquots per well. The membranes were then exposed to 525 nm light using a Modulight ML6600 laser (Modulight USA Inc., San Jose, CA, USA), at a fluence of 11.25 or 90 J/cm^2. The following reference conditions were used: Blank (TBS buffer only), Control (membranes only), Dark effect (membranes + TLD-1433), Light alone (membranes only + light). Lipid peroxidation was measured immediately after the exposure to light.

Lipid peroxidation was determined by measuring the level of malondialdehyde (MDA), a common product of lipid peroxidation, using an MDA assay (CheKine™ Micro Lipid Peroxidation (MDA) Assay Kit, Abbkine, Atlanta, GA, USA). Reaction mix (300 μL) was added to the 100 μL sample in each well, mixed and transferred to Eppendorf tubes that were incubated sealed at 95 °C for 30 min. After that, the tubes were cooled on ice and centrifuged at 10,000×*g* for 10 min at room temperature. The supernatant aliquots (200 μL from each tube) were transferred to a fresh 96-well plate, and absorbance was measured at 535 and 600 nm using a Shimadzu UV 3600 spectrophotometer (Shimadzu Scientific Instruments, Columbia, MD, USA). Absorbance at 600 nm was subtracted from the absorbance at 532 nm, to account for possible sucrose contribution to the overall absorbance. Blank readings were subtracted from all other readings, and MDA concentration [nmol/mL] was calculated in the following way: [MDA] = (Abs_{532} - Abs_{600})/(MEC_{MDA} * pathlength) * reaction volume/sample volume * 10^6; MEC_{MDA} = 155,000 $M^{-1}cm^{-1}$; pathlength = 0.588 cm (based on 0.2 mL volume in a well and 0.34 cm^2 well bottom area); reaction volume = 0.4 mL, and sample volume = 0.1 mL. The data were normalized to control values for each experiment. The experiment was performed in three to four replicates.

2.9. Statistical evaluations

Pairwise comparisons between non-treated and various treatment regimens were evaluated by 2-tailed Student's T-test, with $p \leq 0.05$ considered significant.

3. Results

3.1. Nanomolar concentrations of TLD-1433 inactivate influenza virus, coronavirus and Zika virus

We initially tested the capacity of the Theralase® PDC Ruvidar™ (TLD-1433) to inactivate various model single-stranded (ss) RNA viruses. Sets of each virus were mixed with various concentrations of TLD-1433 and incubated in the dark at room temperature

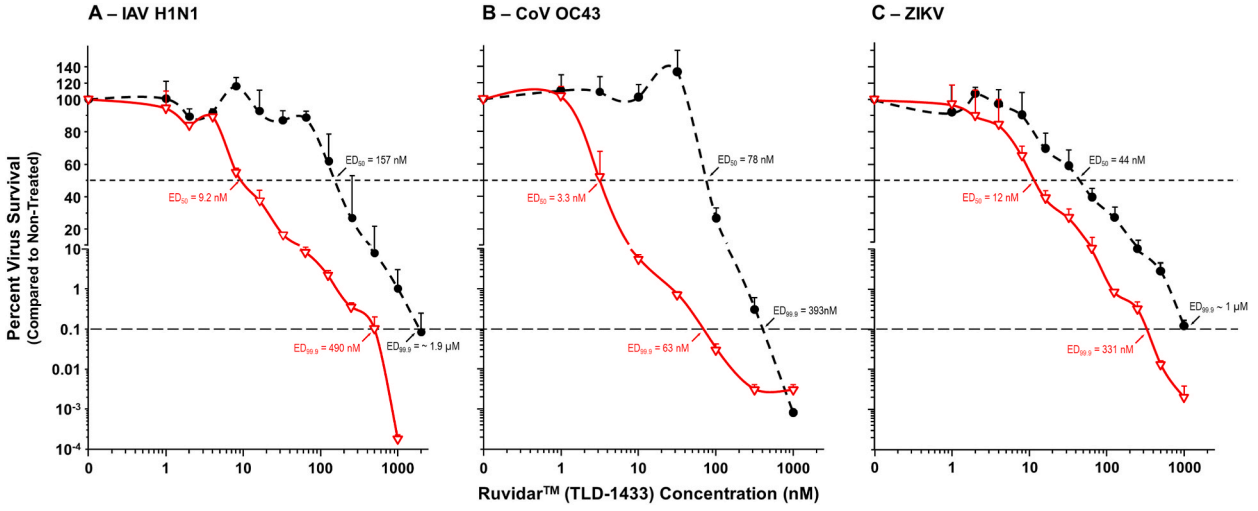

Fig. 2. Planktonic inactivation of influenza A virus (A – IAV H1N1), human coronavirus (B – CoV) OC43 and Zika virus (C – ZIKV). Aliquots of each virus were treated with different concentrations of the Theralase® PDC Ruvidar™ (TLD-1433) and incubated for 30 min. Treated viruses were then either left in the dark (●) or photo-activated with green light at a wavelength of 525 ± 25 nm and an energy density of 45 J/cm^2 for 75 s (red ▽). After an additional "rest" period of 15 min, residual infectivity of each treatment was titrated by either standard plaque assay (IAV H1N1 and ZIKV), or by immuno-focus assay (CoV OC43) and compared to virus treated with no TLD-1433 (set as 100 % for each curve). Values represent the means of at least three replicates. Error bars indicate standard errors of the means (S.E.M.). Effective doses that reduce the virus titers 50 % and 99.9 % (indicated by horizontal dashed lines) are indicated (ED_{50} and $ED_{99.9}$).

(~22 °C) for 30 min. After the 30 min incubation, some sets were maintained in the dark and other sets were exposed to green light in a 96-diode light source (TLD 3000, Theralase™, Inc., Toronto, Ontario), calibrated to deliver 45 J/cm^2 in 75 s. After an additional 15 min incubation at room temperature in the dark, residual virus infectivity was determined. Approximately 50 % of IAV was inactivated by ~120 nM TLD-1433 without photo-activation (Fig. 2a, black dashed curve and horizontal short-dashed line) and nearly 2 μM TLD-1433 was required to inactivate 99.9 % IAV if TLD-1433 was not photo-activated (Fig. 2a, horizontal long-dashed line). When TLD-1433 was photo-activated, 50 % IAV inactivation occurred at ~9 nM TLD-1433, 90 % IAV was inactivated by ~50 nM, 99 % was inactivated by ~170 nM and 99.9 % IAV was inactivated by ~0.5 μM TLD-1433 (Fig. 2a, solid red curve). The OC-43 coronavirus was slightly more sensitive than IAV, requiring ~3 and 8 nM to inactivate 50 and 90 % infectivity, respectively, and 99.9 % inactivation was achieved at ~60 nM (Fig. 2b). ZIKV was slightly less sensitive to photo-activation-mediated inactivation, requiring ~12 and 61 nM to inactivate 50 and 90 % infectivity, respectively, and 99.9 % inactivation was achieved at ~330 nM (Fig. 2c).

3.2. Photo-activated TLD-1433 inactivates tested viruses within seconds

To determine the kinetics of light-activated virus inactivation, we next treated various viruses with a dose of TLD-1433 calculated to inactivate about 99.5 % of each virus (=220 nM), incubated in the dark at room temperature (~22 °C) for 30 min, and then activated the compound by exposing to green light for different periods of time ranging from 5 s to 150 s (=1/25th - 2 × the initial 75 s exposure). Initial results failed to measure any residual hCoV OC-43, so for these, the TLD-1433 concentration was reduced to 16 nM. Results are indicated in Fig. 3.

These results indicate that both IAV and hCoV OC-43 are very rapidly inactivated by brief exposure to light in the presence of the PDC, with >90 % inactivation within about 20 s (Fig. 3a and b). ZIKV appears to be more resistant (Fig. 3c), which also correlates with the observation that higher doses of PDC are required to achieve the same virucidal capacity (Fig. 2c).

We then tested length of time of TLD-1433 pre-incubation before 75 s photo-activation on OC-43 inactivation. These studies were performed at 22 °C (Fig. 4). The extent of OC-43 inactivation was reduced with less than 15 min of exposure, suggesting that the compound required some time to interact with the virus. Since there was little difference if virus was exposed to TLD-1433 for at least 30 min prior to photo-inactivation, we performed subsequent experiments involving light-activation after 30 min TLD-1433 treatment.

We next wondered about the kinetics of virus killing when the PDC was not light-activated. For these experiments, we focused on hCoV OC-43 and incubated aliquots of the virus with various concentrations of PDC for various periods of time (Fig. 5). As seen in earlier results, increasing PDC concentrations, even in the absence of light activation, resulted in increased hCoV killing.

3.3. TLD-1433-mediated inactivation of hCoV OC-43 does not remove the coronavirus spike protein from virus particles

Prior studies of IAV treated with the PDC Zn-PcChol8+ indicated that the influenza HA spike proteins were cleaved off virion particles [27]. To determine whether TLD-1433 caused virus inactivation through a similar mechanism, we treated aliquots of OC43 with 0 or 250 nM TLD-1433 for 30 min, treated with green light and pelleted virion structures at 45,000×*g* for 90 min. Aliquots of the supernatant and pellets were resolved by SDS-PAGE and immuno-probed with an antibody that recognizes the OC43 S protein (Fig. 6).

As expected, all S protein in non-treated samples was found in the pellet. Lack of detectable coronavirus S protein in supernatants from TLD-1433-inactivated coronavirus suggests both that TLD-1433 treatment did not cleave this protein off viral particles, and

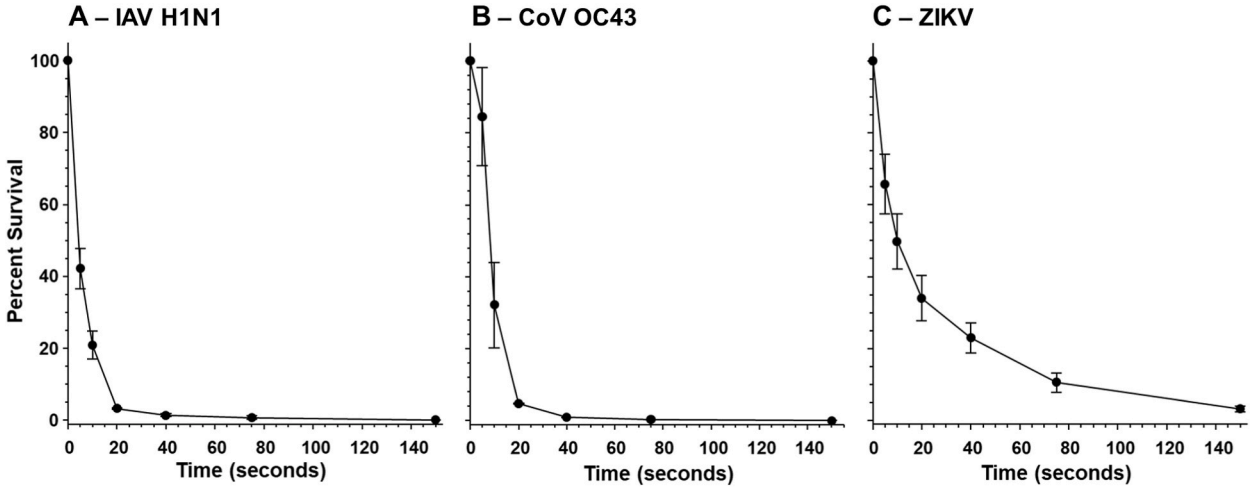

Fig. 3. Kinetics of TLD-1433-mediated virus inactivation. The indicated viruses (**A – IAV H1N1; B – CoV; C – ZIKV**) were treated with 220 nM of TLD-1433 (except CoV OC43, which was treated with 16 nM) for 30 min, then all photo-activated with green light for the indicated times (X-axis), rested 15 min, and residual infectivity determined as described in the legend to Fig. 2. Values represent means of three or more replicates with error bars representing S.E.M.

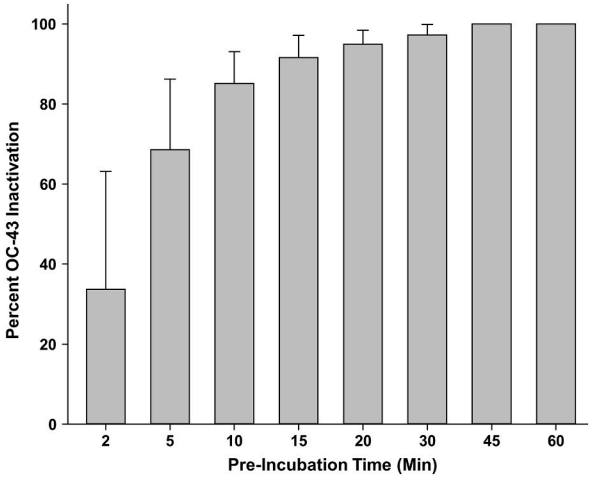

Fig. 4. Effect of pre-incubation time on OC-43 inactivation. Aliquots of OC-43 were mixed with 31.6 nM TLD-1433 and exposed to green light for 75 s after indicated times of incubation at 22 °C. After an additional 15 min rest, residual infectivity was determined. Results are means of triplicate replicates. E.B. = S.E.M.

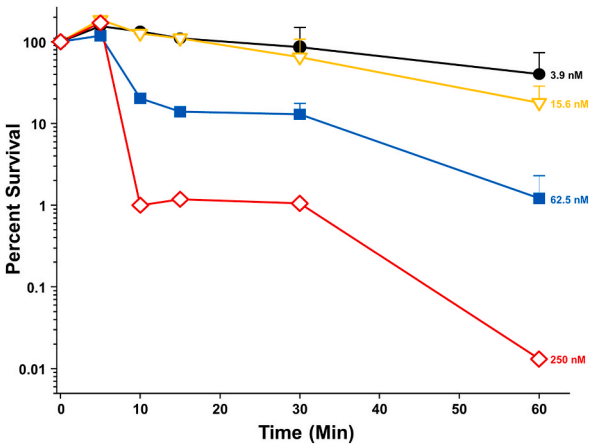

Fig. 5. Kinetics of OC-43 inactivation without light activation. Aliquots of OC-43 were incubated with indicated concentrations of TLD-1433 for indicated amounts of time and residual infectivity titrated. E.B. = S.E.M. from 2 replicates.

detection by antibody suggests little immunologic change in the S protein region(s) recognized by the specific antibody after TLD-1433 treatment.

3.4. *Photo-inactivation is temperature dependent*

While performing these various studies, we noted that OC-43 samples left in the dark at 22 °C had consistently lower titers than virus stocks left on ice and titrated as Controls, even in the absence of TLD-1433. This suggests that hCoV OC-43 is sensitive to

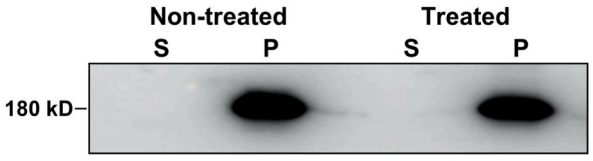

Fig. 6. Antigenicity and location of Spike (S) protein on TLD-1433-treated coronaviruses. Aliquots of CoV OC-43 were either treated with 250 nM TLD-1433 as described in the legend to Fig. 2, or not treated. Virions were pelleted at 40,000×*g* for 90 min and supernatants (S) and virion pellets (P) resolved in SDS-PAGE, then transferred to nitrocellulose and probed with an antibody that recognizes S protein. The complete unaltered blot is shown in Supplementary Fig. S1.

temperatures. To test this, we then incubated aliquots of OC-43 on ice (4 °C), at room temperature (22 °C), or at 37 °C for various periods of time and tested residual infectivity (Fig. 7a).

We also tested the effects of temperature on herpes simplex virus (HSV-1) inactivation since we planned to also determine TLD-1433-mediated inactivation of this double-stranded (ds) DNA virus (Fig. 7b).

These results indicated that inactivation of both viruses was enhanced at elevated temperatures of pre-incubation. They also indicated that hCoV OC-43 is sensitive to temperature fluctuations whereas HSV-1 is not. Since these results indicated that TLD-1433 photo-inactivation of viruses was more effective at 37 °C rather than at room temperature, we pre-incubated mixtures of viruses and TLD-1433 at 37 °C prior to photo-activation in subsequent experiments.

3.5. TLD-1433 also efficiently inactivates herpes simplex virus (HSV-1) and vaccinia virus (VACV), but not adenovirus nor mammalian reovirus

All our prior work had been with enveloped single-stranded (ss)RNA viruses. Virus inactivation could involve any of several different mechanisms, including nucleic acid modification, protein modification and/or lipid modification. To determine whether TLD-1433 also could inactivate viruses with double-stranded (ds) nucleic acid, we tested TLD-1433 effects on Ad5, HSV-1, and VACV, all of which contain dsDNA, and on mammalian reovirus (MRV), which contains dsRNA (Fig. 8).

As with the ssRNA viruses, brief exposure of HSV-1 to nanomolar concentrations of TLD-1433 also resulted in inactivation of this virus (Fig. 8a). Non-activated TLD-1433 inactivated 50 % HSV-1 at 40 nM, inactivated 90 % HSV-1 at 70 nM, and inactivated 99.9 % HSV-1 at 200 nM. Photo-activated TLD-1433 was more efficient, inactivating 50, 90, 99 and 99.9 % HSV-1 at 2.4, 8, 21 and 53 nM, respectively (Fig. 8a; Table 1). Nanomolar concentrations of TLD-1433 also inactivated VACV (Fig. 8b; Table 1). However, the non-enveloped dsDNA virus Ad5, and non-enveloped dsRNA MRV, were not inactivated by TLD-1433 until TLD-1433 concentrations exceeded 1.8 μM if photo-activated and exceeded 8 μM if not photo-activated (Fig. 8c and d; Table 1).

In general, much lower doses of TLD-1433 were required to inactivate the enveloped viruses compared to the non-enveloped viruses. For example, the dose required to inactivate 50 % (ED_{50}) of influenza H1N1 was 117 nM if not light-activated, and 9.2 nM if light-activated. The dose required to inactivate 99.9 % ($ED_{99.9}$) of influenza H1N1 was approximately 2 μM if not light-activated, and approximately 700 nM if light-activated. Similarly, the ED_{50} for HSV-1 was 2.4 nM and the $ED_{99.9}$ was 53 nM if TLD-1433 was light-activated, but the ED_{50} and $ED_{99.9}$ were 40 and 200 nM, respectively, if TLD-1433 was not light-activated. However, the ED_{50} and $ED_{99.9}$ values for non-light-activated inactivation of the non-enveloped adenovirus were about 8.1 and 32 μM, respectively, if not light-activated and 1.8 and 18 μM, respectively, if light-activated. Comparable values for the non-enveloped reovirus were approximately 12 μM and 54 μM, respectively, if not light-activated, and were 5.4 and 47 μM if light-activated, respectively, about 100–1000-fold higher than values needed for most enveloped viruses. Inactivation values for vaccinia virus were intermediate.

3.6. Increased light exposure inactivates more virus

Since the non-enveloped adenovirus and mammalian reoviruses required approximately 100–1000-fold more TLD-1433 to inactivate them than the TLD-1433 dose required to inactivate the enveloped viruses, we tested whether increasing light dosage, rather than TLD-1433 dosage, might inactivate more viruses. Aliquots of stock reovirus were treated with 1, 2, 4 and 8 μM TLD-1433,

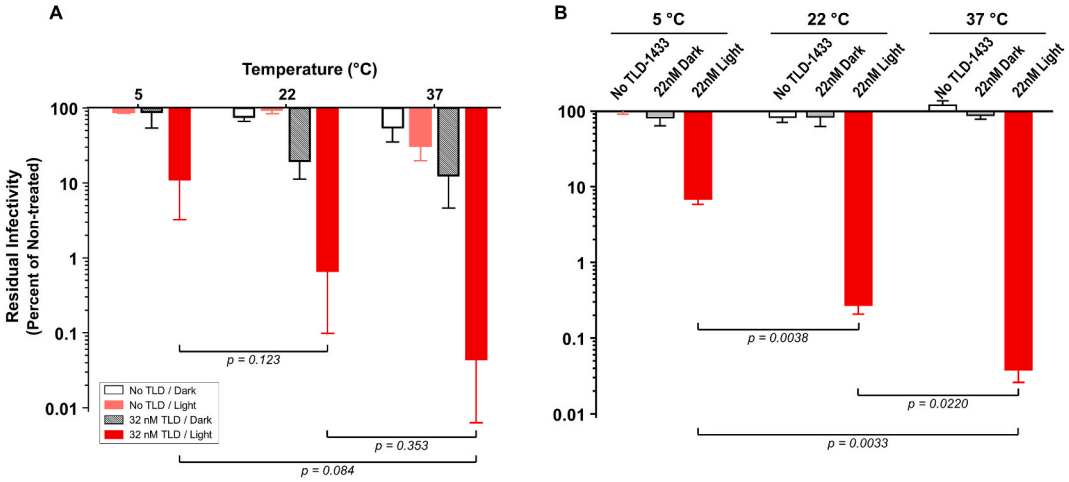

Fig. 7. Pre-incubation temperature effects on virus inactivation. Aliquots of (**A**) CoV OC43 or (**B**) HSV-1 virus were diluted into PBS and treated with 0, 22.5, or 32 nM of the Theralase® PDC TLD-1433 (indicated in legend in **A** and at top of **B**). Reactions were incubated for 30 min at either 5, 22 or 37 °C and exposed to green light for 75 s. Treated viruses were then rested for 15 min and residual infectivity of each determined by immunofocus assay in MRC-5 cells (CoV OC43) or by plaque assay on Vero cells (HSV-1). Values represent the means of at least three replicates. Error bars indicate S.E.M.

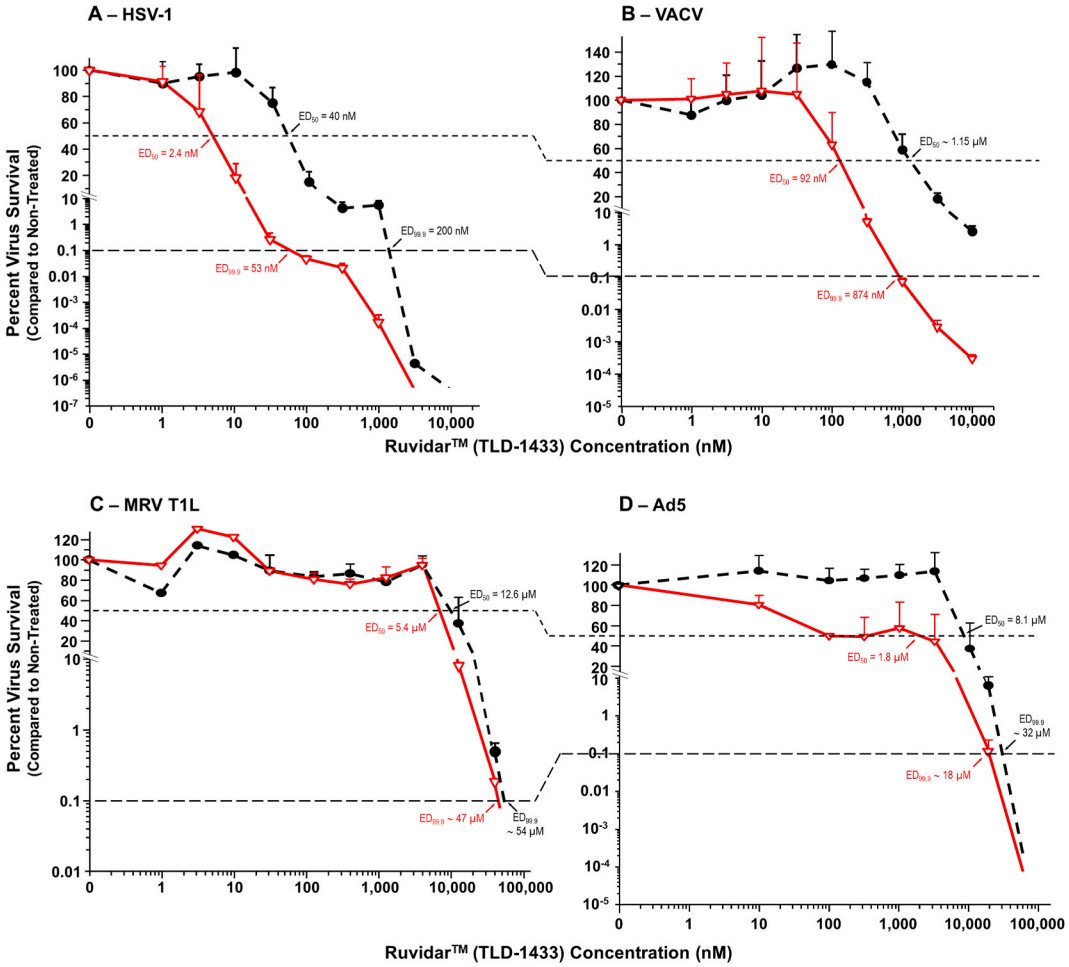

Fig. 8. Planktonic inactivation of herpes simplex, type 1 virus (A – HSV-1), Vaccinia virus (B – VACV), mammalian orthoreovirus type 1 (C – MRV) and Adenovirus type 5 (D – Ad5). Aliquots of each virus were treated with different concentrations of the Theralase® PDC Ruvidar™ (TLD-1433) and incubated for 30 min at 37 °C. Treated viruses were then either left in the dark (●) or photo-activated with green light at a wavelength of 525 ± 25 nm and an energy density of 45 J/cm^2 for 75 s (red ▽). After an additional "rest" period of 15 min, residual infectivity of each treatment was titrated by standard plaque assay in L929 cells (MRV), in A549 cells (Ad5), or in Vero cells (HSV-1 and VACV) and compared to virus treated with no TLD-1433 (set as 100 % for each curve). Values represent the means of at least three replicates. Error bars indicate S.E.M. Effective doses that reduce the virus titers 50 % and 99.9 % (indicated by horizontal dashed lines) are indicated (ED_{50} and $ED_{99.9}$). Lines that end without symbols represent the limit of detection in the assay.

incubated at 37 °C for 30 min, and then exposed to green light for 1–8 cycles of light exposure (=75–600 s; = 90–720 J/cm^2) (Fig. 9).

Increasing light exposure did not have an additive or synergistic effect on virus inactivation at TLD-1433 concentrations of 1–2 μM, but did have additional inactivation effects at ≥ 4 μM.

3.7. *Media components affect TLD-1433-mediated inactivation*

In the course of these studies, we noted variable results for inactivation of some viruses, depending upon stock virus concentration and degree of virus dilution into PBS or various culture media. When concentrated stocks of HSV-1 were diluted into "Complete 2 × Media 199" (M199; media used to dilute agar/agarose for HSV-1, MRV and ZIKV plaque assays) TLD-1433-mediated inactivation of HSV-1 was greatly reduced as compared to when virus was diluted into PBS (Fig. 10).

Whereas dilution of HSV-1 into PBS generally resulted in about a 500-fold reduction in HSV-1 infectivity after photo-activation with 10 nM TLD-1433, and about a 10,000-fold reduction in HSV-1 infectivity after photo-activation with 25 nM TLD-1433 (Fig. 10a), dilution into complete 2 × Media 199 that also contained 6 % FBS, resulted in less than a 3-fold reduction in HSV-1 infectivity after photo-activation (Fig. 10a; compare four left-most bars). Cell culture media contain several components that could potentially affect light-mediated ROS generation, including FBS, phenol red, sodium pyruvate, and many other components.

Thus, we initially tested inactivation in M199 lacking FBS and in PBS supplemented with 6 % FBS (Fig. 10a; 2 right-most bars). Each of these conditions gave intermediate inactivation values, all of which were significantly different from inactivation in PBS alone.

Table 1
Ruvidar™ doses required to inactivate indicated percentages of indicated viruses.

			Effective dose (nM) to inhibit indicated viruses[a]			
Virus	Virus Characteristics	Treatment	ED_{50}	ED_{90}	ED_{99}	$ED_{99.9}$
Coronavirus	Single-stranded (ss) RNA; Enveloped	Dark	78 ± 7.5	128 ± 8	232 ± 46	393 ± 107
		Light	3.3 ± 0.9	6.7 ± 1.0	23 ± 1.2	63 ± 4.6
Herpesvirus	Double-stranded (ds) DNA; Enveloped	Dark	40 ± 18	70 ± 20	126 ± 20	200 ± 32
		Light	2.4 ± 0.2	8 ± 1.9	21 ± 5.4	53 ± 18.4
Influenza virus	Single-stranded (ss) RNA; Enveloped	Dark	157 ± 83	460 ± 217	1920 ± 547	n.d.[b]
		Light	9.2 ± 1.6	53 ± 5.5	168 ± 48	490 ± 78
Vaccinia virus	Double-stranded (ds) DNA; Enveloped	Dark	1147 ± 307	4574 ± 826	7987 ± 1707	n.d.
		Light	92.3 ± 32.1	216 ± 26	462 ± 16.6	874 ± 91.6
Zika virus	Single-stranded (ss) RNA; Enveloped	Dark	44 ± 7.1	237 ± 53	628 ± 114	n.d.
		Light	12.0 ± 2.6	61 ± 11.5	117 ± 27	331 ± 150
			Effective dose (μM) to inhibit indicated viruses[a]			
			ED_{50}	**ED_{90}**	**ED_{99}**	**$ED_{99.9}$**
Adenovirus	Double-stranded (ds) DNA; Non-enveloped	Dark	8.1 ± 3.5	17 ± 8.4	23 ± 9	32 ± 11
		Light	1.8 ± 0.9	6.2 ± 3.8	11 ± 6	18 ± 9
Reovirus	Double-stranded (ds) RNA; Non-enveloped	Dark	12.6 ± 1.5	20 ± 0.8	34 ± 2	54 ± 6
		Light	5.4 ± 0.26	11 ± 1.3	25 ± 0.1	47 ± 0.6

[a] Effective doses (ED) values determined from a minimum of 3 replicates. Values compiled from data depicted in Figs. 2 and 8. ± indicates in Figs. 2 and 8. ± indicates S.E.M.
[b] Not determined; above tested dose.

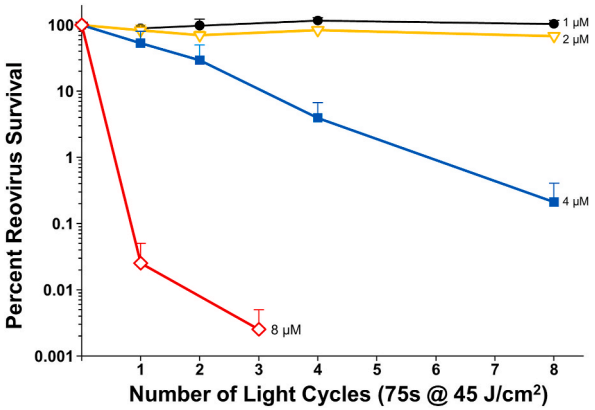

Fig. 9. Effect of light exposure on reovirus survival. Aliquots of reovirus were treated with the indicated concentrations of Ruvidar® (TLD-1433), incubated at 37 °C for 30 min, exposed to green light for the indicated numbers of 75 s cycles, rested for 5min between each cycle and for a final period of 15min, and residual infectivity determined. Error bars indicate S.E.M. from at least two replicates.

We then examined effects of diluting HSV-1 into either DMEM or M199 of different concentrations (Fig. 10b). There were minor alterations in TLD-1433-mediated inactivation in DMEM of different strengths, but significant alterations in TLD-1433-mediated inactivation in M199 of different strengths. For example, there was a 249-fold difference ($p = 0.042$) in inactivation when comparing 2 × M199 to PBS (Fig. 10c). Furthermore, as before, addition of FBS (2 × M199+) led to an even greater fold-change in inactivation.

DMEM and M199 contain different amounts of phenol red, and such a red dye might interfere with green light transmission. Thus, we then checked the effect of phenol red, both by altering the volume (depth of solution) and the concentration of phenol red in which the inactivation studies were performed (Fig. 11). Although altering the PBS volume had no effect on inactivation, increasing the volume of phenol red-containing media led to increases in residual infectivity (Fig. 11a), although these differences were not statistically significant. Maintaining a constant volume of 100 μL, but changing the concentration of phenol red during inactivation, led to significant changes in TLD-1433-mediated HSV-1 inactivation (Fig. 11b and c). For example, there were >2000- and >9000-fold alterations in inactivation when comparing PBS that contained 8 × (160 mg/mL) phenol red compared to none, or only 0.5 × phenol red.

FBS contains anti-oxidants such as ascorbic acid, tocopherols, beta-carotene, superoxide dismutase, catalase, glutathione, uric acid, and polyphenols [28]. Therefore, we extended the above FBS conditions by examining different concentrations (Fig. 12a, left). There was a clear dose response effect depending upon amount of FBS present in the virus-containing solution prior to and during TLD-1433-mediated inactivation (Fig. 12b, left). Thus, in subsequent studies we keep FBS concentrations to a minimum.

Cell culture media also contains sodium pyruvate, a peroxide scavenger [29]. Thus, we also added different concentrations of

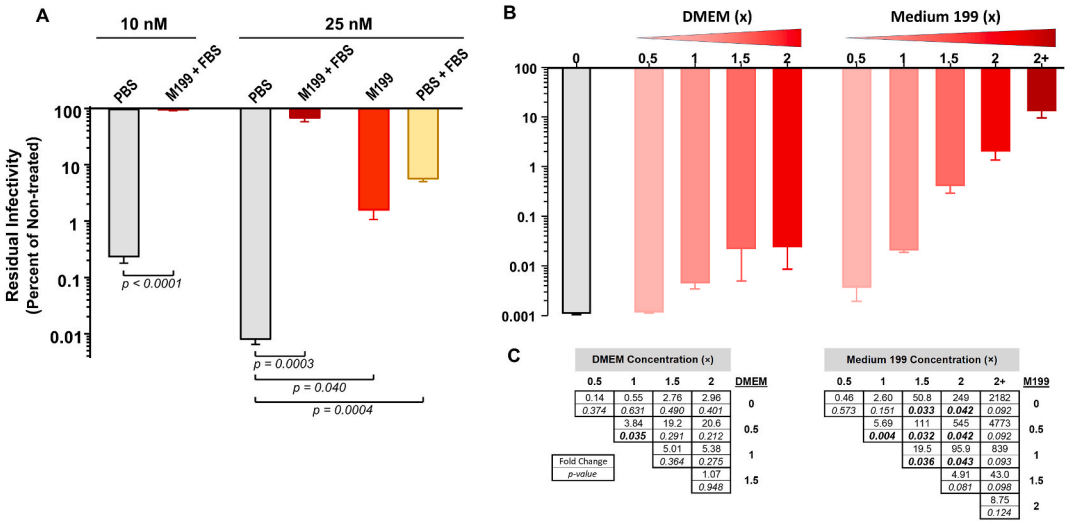

Fig. 10. Differential media effects on HSV-1 inactivation. Aliquots of virus were diluted >50-fold into (**A**) either PBS or indicated media ± FBS and treated with 10 or 25 nM of TLD-1433 (indicated at top); or (**B**) into PBS (left-most white bar) or into indicated concentrations of DMEM or Medium 199 and treated with 22.5 nM TLD-1433. Reactions were incubated for 30 min at 37 °C, treated with green light for 75 s, treated viruses rested for 15 min, and residual infectivity determined by plaque assay on Vero cells. Values represent the means of at least three replicates. Error bars indicate S.E.M. **C.** Fold-changes (upper value in each box) and p-values (lower italicized values in each box) of each indicated pairwise comparison. Larger bolded p-values are statistically significant by Student's T-test.

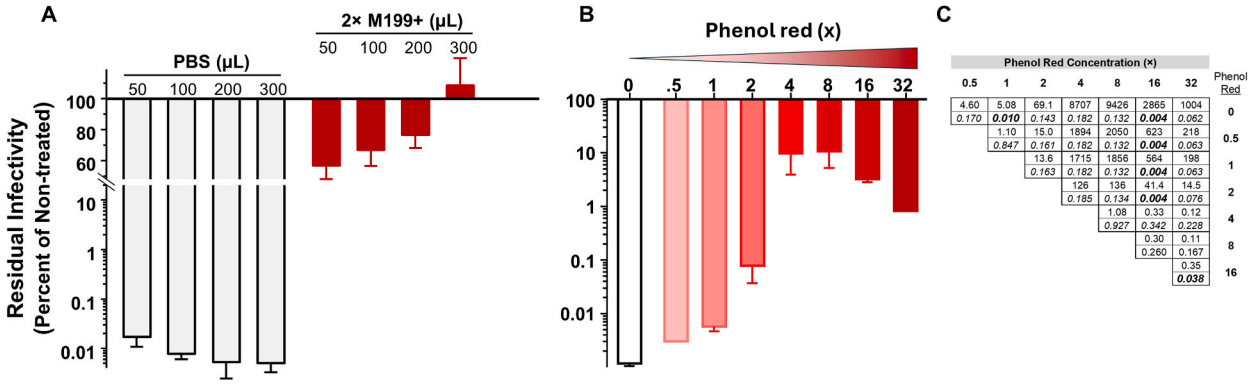

Fig. 11. Phenol red effects on HSV-1 inactivation. Aliquots of virus were diluted >50-fold into either PBS (white bar at left) or into indicated concentrations of DMEM or Medium 199 and treated with 22.5 nM of TLD-1433. Reactions were incubated for 30 min at 37 °C and exposed to green light for 75 s. Treated viruses were then rested for 15 min and residual infectivity of each determined by plaque assay on Vero cells. 2+: 2 × Medium 199 supplemented with 6 % FBS. Values represent the means of at least three replicates. Error bars indicate S.E.M.

sodium pyruvate into HSV-1 that had been diluted into PBS (Fig. 12a, right). Differences in sodium pyruvate concentrations had little effect on TLD-1433-mediated inactivation of HSV-1 (Fig. 12b, right).

Similarly, some of the virus concentration procedures described earlier result in stock viral solutions with visible turbidity. For example, concentrated VACV solutions may have turbidity similar to that of ~33 % milk, as measured by OD_{440}. Thus, we made serial dilutions of stock VACV to turbidities equivalent to ≈0.1 % milk, and treated these dilutions with TLD-1433 (Fig. 13). TLD-1433-mediated inactivation was more effective when turbidity was less than that equivalent to ~1 % milk. Furthermore, at solution turbidity < ~0.6 % milk, there is >90 % VACV inactivation, and this inactivation increases rapidly to >99 % at turbidity < ~0.3 % milk (Fig. 13a and b).

The dramatic difference in capacity for TLD-1433 to inactivate enveloped viruses compared to the tested non-enveloped viruses suggests that some modification of the viral lipid membrane may be accounting for virus inactivation. We then tested the capacity of TLD-1433 ± light-activation to generate singlet oxygen (Fig. 14a) and hydroxyl radicals (Fig. 14b), and to peroxidate membrane lipids (Fig. 14c).

Dark treatment, and light treatment in the absence of TLD-1433, generated no significant increase in lipid peroxidation compared to control membranes. Light-activation caused a dose-dependent increase in TLD-1433-mediated lipid peroxidation, with a 2.3-fold

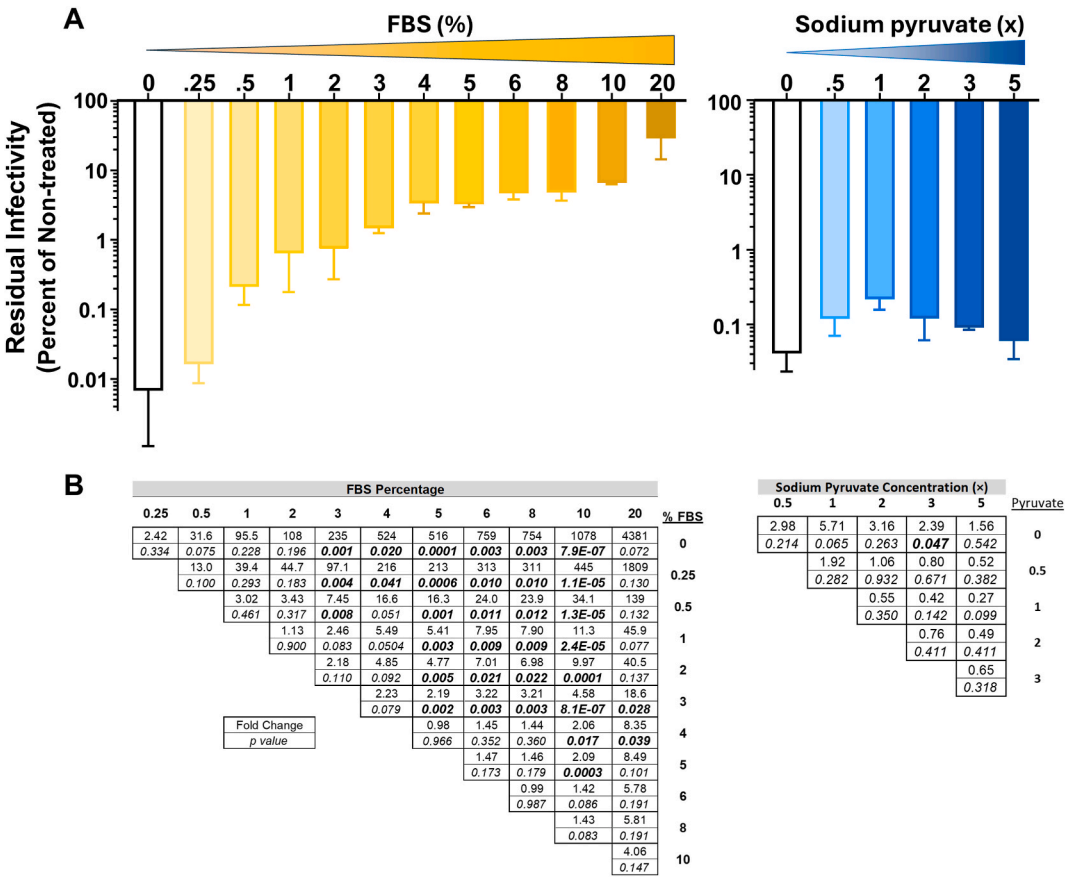

Fig. 12. Media component effects on HSV-1 inactivation. Aliquots of virus were diluted >50-fold into either PBS (white bar at left) or into indicated concentrations of DMEM or Medium 199 and treated with 22.5 nM of TLD-1433. Reactions were incubated for 30 min at 37 °C and exposed to green light for 75 s. Treated viruses were then rested for 15 min and residual infectivity of each determined by plaque assay on Vero cells. 2+: 2 × Medium 199 supplemented with 6 % FBS. Values represent the means of at least three replicates. Error bars indicate S.E.M.

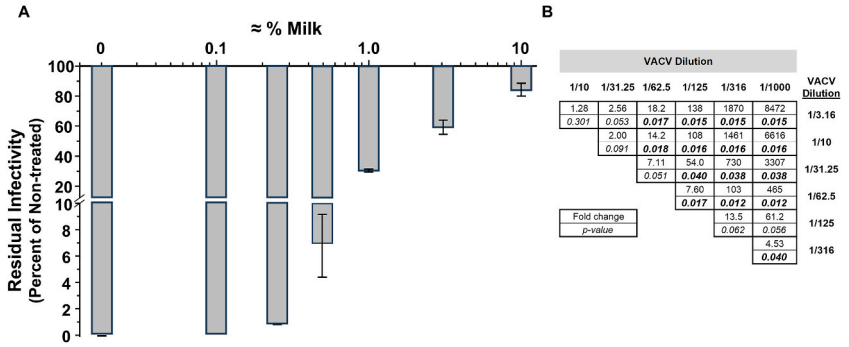

Fig. 13. Virus turbidity effects on VACV inactivation. Aliquots of a concentrated stock of VACV (≈32 % milk turbidity) were diluted 3- to 1000-fold into PBS. Reactions were treated with 1 μM of the Theralase® PDC TLD-1433. Reactions were incubated for 30 min at 37 °C, irradiated for 75 s, rested for 15 min and residual infectivity determined by plaque assay on Vero cells. Values represent the means of at least three replicates. Error bars indicate S.E.M.

increase in lipid peroxidation at 11.25 J of energy and about 5-fold at 90 J of energy.

To use the TLD-1433 technology as a means to completely inactivate a pathogenic virus; for example as a method to generate a wholly-inactivated vaccine from a known virus(es), would require the absence of any infectious virus after the procedure. To test this, we treated highly concentrated HSV-1 with TLD-1433 and inoculated the treated virus onto monolayers of Vero cells. We also inoculated known PFU, as controls. We monitored CPE over several passages (Table 2). Cells inoculated with ≥2 PFU of HSV-1

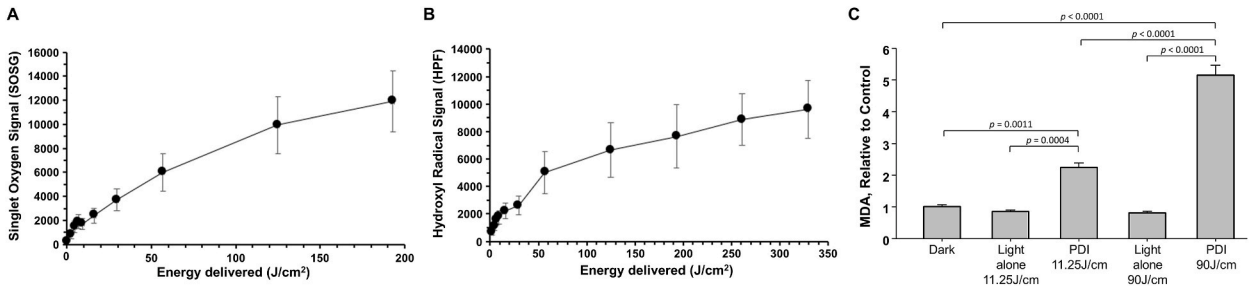

Fig. 14. A. TLD-1433-mediated ROS and (B) Hydroxyl radical generation. ROS and hydroxyl radical generation by 3 μM TLD-1433 in DMEM (not supplemented with FBS) under 535 nm light (227 mW/cm^2). Error bars indicate S.E.M. from 5 to 7 replicates. **C. Lipid peroxidation of A549 membranes.** Purified A549 cell membranes were treated as indicated and amounts of lipid peroxidation, compared to non-treated control cell membranes, determined by MDA kit. Values represent averages from three or more replicates with error bars indicating S.E.M.

demonstrated CPE by the 2nd passage. Similarly, cells inoculated with virus treated with 1.0 μM TLD-1433 and irradiated for 75 s also showed CPE by the 2nd passage. Half of the cell monolayers inoculated with 1 PFU of HSV-1 showed CPE during the 2nd and 3rd passages, similar to Poisson distribution predictions. The sample treated with 1.0 μM TLD-1433 and irradiated for 150 s showed minimal CPE by the end of the 2nd passage but showed clear CPE during the 3rd passage. However, cells inoculated with no virus, and those inoculated with virus treated with ≥3.16 μM TLD-1433, demonstrated no CPE, even after three passages, indicating no infectious virus after these treatments.

4. Discussion

Infectious agents, including viruses, remain a major cause of morbidity and mortality worldwide. Vaccines remain a front-line means to combat infectious agents, but they require months to years to develop, are highly specific and normally must be applied weeks before exposure to allow immunity to develop. Anti-viral pharmacologic compounds are another strategy used to combat infectious agents. For example, ribavirin is a broad-spectrum anti-viral that has some effect against many viruses [30–33]. Another broad-spectrum compound is mycophenolic acid [34–36]. Many of these pharmacologic compounds are effective in the high micromolar to low millimolar range.

PDT is an alternate strategy that has been demonstrated effective against various cancers [9,10,12], against bacterial pathogens [14,15] and against viruses [17,19,20,37]. PDT is based upon use of a PDC, which is activated by exposure to specific wavelengths of light to produce ROS/singlet oxygen, which effect microbial or cancer killing [15,18]. Hence, PDT utilizes PDC, light and oxygen to destroy tumors and pathogens with an induction of an antigen-specific immune response [38,39]. PDT is delivered by local or systemic administration of a PDC (at a non-toxic dose) and subsequent exposure to light, which activates the PDC. The presence of oxygen in the treatment target is not a delivered, but an intrinsically present component, although the requirement for oxygen can be an impedance in hypoxic targets. However, TLD-1433 has been demonstrated to be effective in low oxygen environments. Importantly, PDT-induced toxicity occurs only in regions where all three treatment components are present simultaneously, which reduces any collateral damage to normal tissues, where the PDC and/or light exposure is absent. Upon photon absorption, the PDC enters a singlet excited state resolving to the reactive triplet state via inter system crossing (ISC). The triplet state then energetically relaxes by producing ROS: highly reactive and cytotoxic singlet oxygen ($^1O_2$) generated by energy transfer to stable triplet oxygen (type II photoreaction) and/or electron transfer to oxygen (type I photoreaction) generating superoxide radical (O2•-), hydrogen peroxide (H_2O_2) and eventually very reactive hydroxyl radical (•OH). A number of different PDCs have been developed and tested (reviewed in Refs. [12,21]).

TLD-1433 is a ruthenium(II)-based PDC marketed by Theralase®. It represents a complex with the formula [Ru(II)(4,4′-dmb)$_2$(IP-3T)]Cl$_2$, where 4,4′-dmb = 4,4′-dimethyl-2,2′-bipyridine; IP = imidazo [4,5], [1,10]phenanthroline; 3T = α-terthienyl (oligomer consisting of three tyophenes) (Fig. 1a). It is the first ruthenium-based PDC that has advanced to clinical studies and is under investigation to treat BCG-unresponsive NMIBC CIS with PDT. TLD-1433 as a metal complex differs from more conventional macrocyclic, pyrrole-containing PDCs (such as Photofrin®) and is unique in its photosensitizing mechanism and efficacy. In terms of its photophysics and photochemistry, TLD-1433 is a dyad complex comprising an essential Ru(II) central metal ion and the 3T chromophoric ligand (complexed with the central ion via IP tether). The central Ru(II) ensures photon absorption with fast and efficient charge transfer to the 3T ligand and ISC of singlet excited state to triplet excited state (almost unity efficiency), with little loss to luminescence emission. The extended aromatic structure of the 3T ligand, in turn, ensures 3T-localized triplet excited states (intraligand 3IL and intraligand charge transfer 3ILCT) that have significant ππ* character. 3T excitation states are energetically low-lying and hence have unusually prolonged lifetimes. This allows a possibility of both types of photoreactions: energy transfer producing $^1O_2$ at very high quantum yield and electron transfer producing very reactive free radicals (Fig. 1b). Moreover, the excited 3T ligand is uniquely flexible in switching between energy transfer and electron transfer reactions [40,24]. This dyad character of TLD-1433 distinguishes it from other non-dyad Ru (II) complexes as well as from the free IP-3T ligand. The highly photosensitizing 3IL/3ILCT states can be accessed with green light [12,24].

TLD-1433 is effective against Gram-negative *E. coli* [23], and against Gram-positive *S. aureus* and *MRSA* [14]. Arenas and colleagues demonstrated that TLD-1433 was effective in killing *S. aureus* and *MRSA* at dosages ~1000-fold lower than methylene blue

Table 2
Cytopathic effect (CPE) induced by TLD-1433-treated HSV-1.

			Cytopathic Effect (CPE) induced during										
Virus Inoculum			**1st passage**				**2nd passage**					**3rd passage**	
Known[#]	**# Replicates**		**3[@]**	**4**	**5**	**6**	**2**	**3**	**4**	**5**	**6**	**3**	**6**
1000	**1**		+	+	++	+++	+++	++++	++++	++++	++++		
100	**1**		–	–	+	++	+++	++++	++++	++++	++++		
10	**1**		–	–	–	+/–	++	+++	++++	++++	++++		
4	**2**		–	–	–	–	+	++	+++	++++	++++		
2	**6**		–	–	–	–	++++ (3/6) ++ (2)–(1)	++++ (5/6) - (1)	++++ (5/6) - (1)	++++ (5/6) - (1)	++++ (5/6) - (1)		
1	**6**		–	–	–	–	++++ (1/6) + (1)–(4)	++++ (2/6) + (1)–(3)	++++ (2/6) + (1)–(3)	++++ (2/6) ++ (1)–(3)	++++ (2/6) ++ (1)–(3)	++++ (3/6) - (3/6)	++++ (3/6) - (3/6)
0	**6**		–	–	–	–	–	–	–	–	–	–	–
TLD-1433 Treatment	**Estimated virus***	**Light Treatment[&]**											
31.6 nM	**18,500**	**1**	+	+	++	+++	+++	++++	++++	++++	++++		
316 nM	**230**	**1**	–	–	+	+	++	+++	++++	++++	++++		
1.0 µM	**25**	**1**	–	–	–	–	++	++++	++++	++++	++++	++++	++++
		2	–	–	–	–	–	–	–	+/–	+/–	+++	++++
3.16 µM	**< 1**	**1**	–	–	–	–	–	–	–	–	–	–	–
		2	–	–	–	–	–	–	–	–	–	–	–
10 µM	**< 1**	**1**	–	–	–	–	–	–	–	–	–	–	–

10 cm2 well inoculated with known amount of infectious HSV-1. 0 = Mock-infected. +/–: ~5 % CPE.
Number refers to day post-inoculation. + : 5–10 % CPE.
Estimated amount of infectious post-treated HSV-1 based upon starting titer and back-calculated from killing curve (Fig. 8c). ++: 10–30 % CPE.
Number of 75s light cycles. +++: 30–80 % CPE ++++: >95 % CPE.

[14]. TLD-1433 also is clinically used against several cancers [9]. Given its current usage and effectiveness against bacteria, we tested whether it also was effective against several human pathogenic viruses. We found that nanomolar concentrations of TLD-1433 were effective in inactivating >99 % of IAV, human CoV OC-43, Zika virus and herpes virus (Figs. 2 and 8). Inactivation was very rapid; it required only seconds of exposure to light activation (Fig. 3).

TLD-1433-mediated PDT also did not appear to disrupt antigenic epitopes recognized by a single tested antibody on a tested human coronavirus (Fig. 5). The continued recognition of coronavirus S protein on PDT-treated coronavirus, and lack of any detectable S protein in the reaction supernatant after treatment indicates that the coronavirus spike protein remained particle-associated. Furthermore, coronavirus spike protein region(s) recognized by the antibody remained antigenically indistinguishable from those on non-treated virus particles. This, in turn, suggests that TLD-1433-mediated PDT may be a highly effective method for producing inactivated whole-virus vaccines to combat current and future pandemics, although further testing of the immunogenicity of PDT-treated entire spike protein is needed to validate this supposition.

Several parameters affect the efficiency of TLD-1433-mediated inactivation. Even in the absence of light-activation, there is a dose-response capacity of the compound to inactivate every tested virus. This ranged generally from mid-to high-nanomolar concentrations for the enveloped viruses, with VACV being a notable exception, to low micromolar concentrations for the non-enveloped viruses. When TLD-1433-treated enveloped viruses were light-activated, the ED_{50} ranged from a low of 2.4 nM for HSV-1 to a high of 12 nM for Zika virus (and 92 nM for VACV). The corresponding $ED_{99.9}$ ranged from a low of 53 nM for HSV-1 to a high of 490 nM for Influenza virus (and 874 nM for VACV). The corresponding ED_{50} and $ED_{99.9}$ for the non-enveloped viruses were ~8–12 μM and ~32–54 μM if not light-activated, and ~2–5 μM and ~18–47 μM if light-activated. These results suggested that the lipids in the enveloped viruses may influence virus inactivation and peroxidation analyses of membranes (Fig. 12) support this concept.

VACV membranes are incorporated into virions by a distinct mechanism. Influenza virus acquires its membrane as newly formed ribonucleoprotein complexes bud through the plasma membrane (reviewed in Refs. [41,42]). Coronaviruses and Zika virus acquire their membranes as they bud into intracellular vesicles during maturation (reviewed in Refs. [43–46]). Herpes viruses acquire their membranes either by budding though the nuclear membrane (and then losing one of the membranes), or by gaining, losing, and re-gaining a single membrane (reviewed in Refs. [47,48]). Conversely, VACV is believed to acquire its membrane by sequestering lipids from intracellular organelles ([49,50]). This may explain VACV's distinctly different and intermediate TLD-1433 concentration-dependent inactivation profile compared to the other viruses.

FBS has a dramatic effect on efficiency of TLD-1433-mediated inactivation. This could have played a role in the apparent higher doses of TLD-1433 required to inactivate ZIKV compared to the other non-enveloped viruses. Both influenza virus and coronaviruses are efficiently grown in media lacking FBS, but supplemented with trypsin to activate their cell-attachment proteins. However, all other tested viruses are most efficiently grown in media supplemented with 6–10 % FBS. The preparation of high-titer Ad5, HSV-1 and MRV involved some pelleting steps and/or cell washing that removed FBS. ZIKV preparations were routinely diluted 2 – 6-fold into PBS, but there could have been residual FBS that could have affected the apparent doses required to inactivate this virus.

Conditions that interfere with light transmission also play a role in efficiency of light-activation. These included depth of, and concentrations of, phenol red (a dye that absorbs green light) and solution turbidity. Thus, for most of these reported studies, the reaction volumes were kept to 65–70 μL in each well of the 96-well plates. While cellular mechanisms of ROS-induced damage have been extensively studied, it remains unclear whether ROS-based lipid modification can be used to inactivate viruses and induce anti-viral immune responses. Lipids are a major component of membrane-enveloped viruses, which plays an important role in merging two initially distinct lipid bilayers into a single lipid bilayer, thus enabling fusion of viral and cell membranes for viral entry [51]. It is well known that ROS can damage lipid molecules. Singlet oxygen can attack unsaturated lipids causing their peroxidation and change in membrane properties [52]. In addition, hydroxyl (•OH) and superoxide (O2•-) radicals cause lipid peroxidation by attacking hydrogen atoms in the fatty acid chains of lipids. The hydroxyl radical is considered the most aggressive and chemically destructive ROS, with lifetime (and therefore diffusion distance) considerably longer than that of $^1O_2$. Furthermore, lipid peroxidation may self-propagate through a chain reaction: the lipid radicals produced by ROS can promote further formation of lipid peroxyl radicals (ROO•) and eventually of lipid hydroperoxides (LOOH) and various secondary products. Decomposition of lipid hydroperoxides includes such products as aldehydes, most notably malondialdehyde (MDA) and 4-hydroxynonenal (4-HNE). Besides disruption of the lipid bilayer, these highly reactive aldehydes can cause further oxidative damage to neighboring proteins [53].

TLD-1433 is capable of generating ROS (both $^1O_2$ and •OH) in solution upon exposure to green light (Fig. 14). Therefore, we hypothesized that exposure to ROS might provide an attractive method to generate effective inactivated virus vaccines (enveloped but potentially non-enveloped also). The obtained results indicate that TLD-1433 can peroxidize lipids in cell-derived membranes (1 μM TLD-1433, 11.25 J/cm^2 at 535 nm). As enveloped viruses obtain their membranous envelopes from host cells, this activity of TLD-1433 can explain its anti-viral effect that is stronger in enveloped viruses. Moreover, the PDT-induced lipid peroxidation was dose-dependent, which suggests potential for greater damage at increased light energy delivery. Furthermore, ROS-induced lipid peroxidation in the viral envelope and subsequent disruption of the viral membrane structure can potentially inhibit the fusion of the viral envelope and the target cell membrane and hence cell infection.

Importantly, the lipid-targeting TLD-1433 PDT as a virus inactivation strategy is not susceptible to provoking evolution of viral resistance to antiviral treatment. The envelope is not encoded by the viral genome and is not produced during intracellular virus replication, but is inherited from the host cell. This circumstance is especially important for the population of immunocompromised patients, who have ongoing viral replication and prolonged anti-viral drug exposure. The latter presents an increasing concern of selection of strains resistant to further treatment. Hence, TLD-1433 PDT, as a novel ROS-dependent virus inactivation strategy, could be a putative alternative to current agents such as formalin for the preparation of inactivated vaccines. As mentioned above, the inactivation of coronavirus by TLD1433 PDT-induced ROS did not affect the availability of viral surface proteins responsible for

immune recognition.

In the absence of a lipid envelope, the antiviral efficacy of TLD-1433-PDT can be explained by targeting molecules other than lipids. For example, it is known that other Ru (II) complexes that differ from TLD-1433 due to the lack of methylation of bipyridines can bind to plasmid DNA (without intercalation) and photocleave it after exposure to light, producing double-strand breaks; the latter potency may be unique to oligothiophene dyads among Ru(II) complexes. Moreover, this DNA cleaving activity occurred even after scavenging of ROS: singlet oxygen, hydrogen peroxide, hydroxyl radical, and superoxide anion [40]. Hence, the viral inactivation mediated by TLD-1433-PDT-induced ROS is effective against different families of viruses, not only enveloped but also non-enveloped, via lipid peroxidation and potentially other mechanisms. Immune recognition structures appear to remain intact during this inactivation. This opens potential opportunity to generate a broad spectrum of inactivated virus(es) vaccines with greater potency than vaccines produced by currently available inactivation techniques.

Funding

This research was supported by funding provided by Theralase® Technologies, Inc. to K.M.C.

Ethics statement

- Review and/or approval by an ethics committee was not needed for this study because none of the work involved live subjects, either human or animal.
- Informed consent was not required for this study because no patient data were collected.

Data availability statement

Most of the data are available in all Tables and Figures of the manuscript. Moreover, the data are available on request.

CRediT authorship contribution statement

Kevin M. Coombs: Writing – review & editing, Writing – original draft, Visualization, Supervision, Project administration, Investigation, Funding acquisition, Formal analysis, Conceptualization. **Kathleen K.M. Glover:** Writing – review & editing, Visualization, Investigation. **Raquel Russell:** Writing – review & editing, Investigation. **Pavel Kaspler:** Writing – review & editing, Investigation, Formal analysis. **Mark Roufaiel:** Writing – review & editing, Investigation, Formal analysis. **Drayson Graves:** Writing – review & editing, Investigation, Formal analysis. **Peter Pelka:** Writing – review & editing, Supervision, Investigation, Formal analysis. **Darwyn Kobasa:** Writing – review & editing, Conceptualization. **Roger DuMoulin-White:** Writing – review & editing, Conceptualization. **Arkady Mandel:** Writing – review & editing, Supervision, Formal analysis, Conceptualization.

Declaration of competing interest

The authors declare the following financial interests/personal relationships which may be considered as potential competing interests:Kevin M Coombs reports financial support was provided by Theralase Technologies Inc. None If there are other authors, they declare that they have no known competing financial interests or personal relationships that could have appeared to influence the work reported in this paper.

Acknowledgments

This research was supported by funding provided by Theralase® Technologies, Inc. to K.M.C.

Appendix A. Supplementary data

Supplementary data to this article can be found online at https://doi.org/10.1016/j.heliyon.2024.e32140.

References

[1] I. Celik, E. Saatci, F.O. Eyuboglu, Emerging and reemerging respiratory viral infections up to Covid-19. Turk, J. Med. Sci. 50 (2020) 557–562. https://doi:10.3906/sag-2004-126.
[2] J. Zheng, SARS-CoV-2: an emerging coronavirus that causes a global threat, Int. J. Biol. Sci. 16 (2020) 1678–1685. https://doi:10.7150/ijbs.45053.
[3] S.B. Zaman, et al., A review on antibiotic resistance: alarm bells are ringing, Cureus 9 (2017) e1403. https://doi:10.7759/cureus.1403.
[4] J.C. de Jong, et al., Mismatch between the 1997/1998 influenza vaccine and the major epidemic A(H3N2) virus strain as the cause of an inadequate vaccine-induced antibody response to this strain in the elderly, J. Med. Virol. 61 (2000) 94–99. PMID:10745239.
[5] M.C.W. Chan, et al., Frequent genetic mismatch between vaccine strains and circulating seasonal Influenza viruses, Hong Kong, China, 1996-2012, Emerg. Infect. Dis. 24 (2018) 1825–1834. https://doi:10.3201/eid2410.180652.

[6] A.S. Monto, et al., Detection of influenza viruses resistant to neuraminidase inhibitors in global surveillance during the first 3 years of their use, Antimicrob. Agents Chemother. 50 (2006) 2395–2402. https://doi:10.1128/AAC.01339-05.
[7] P.M. Colman, New antivirals and drug resistance, Annu. Rev. Biochem. 78 (2009) 95–118. https://doi:10.1146/annurev.biochem.78.082207.084029.
[8] E. Krol, M. Rychowska, B. Szewczyk, Antivirals - current trends in fighting influenza, Acta Biochim. Pol. 61 (2014) 495–504. https://doi:10.18388/ABP.2014_1870.
[9] J. Fong, et al., A novel class of ruthenium-based photosensitizers effectively kills in vitro cancer cells and in vivo tumors, Photochem. Photobiol. Sci. 14 (2015) 2014–2023. https://doi:10.1039/c4pp00438h.
[10] S. Lazic, et al., Photodynamic therapy for non-muscle invasive bladder cancer mediated by instilled photosensitizer TLD1433 and green light activation, J. Urol. 195 (2016) E805, https://doi.org/10.1016/j.juro.2016.02.880. E805.
[11] J.A. Roque, et al., Breaking the barrier: an osmium photosensitizer with unprecedented hypoxic phototoxicity for real world photodynamic therapy, Chem. Sci. 11 (2020) 9784–9806. https://doi:10.1039/d0sc03008b.
[12] S.A. McFarland, et al., Metal-based photosensitizers for photodynamic therapy: the future of multimodal oncology? Curr. Opin. Chem. Biol. 56 (2020) 23–27. https://doi:10.1016/j.cbpa.2019.10.004.
[13] P. Konda, et al., Discovery of immunogenic cell death-inducing ruthenium-based photosensitizers for anticancer photodynamic therapy, OncoImmunology 10 (2021) 1863626. https://doi:10.1080/2162402X.2020.1863626.
[14] Y. Arenas, et al., Photodynamic inactivation of Staphylococcus aureus and methicillin-resistant Staphylococcus aureus with Ru(II)-based type I/type II photosensitizers, Photodiagnosis Photodyn. Ther. 10 (2013) 615–625. https://doi:10.1016/j.pdpdt.2013.07.001.
[15] M. Klausen, M. Ucuncu, M. Bradley, Design of photosensitizing agents for targeted antimicrobial photodynamic therapy, Molecules 25 (2020) 5239. https://doi:0.3390/molecules25225239.
[16] J.F. Papin, R.A. Floyd, D.P. Dittmer, Methylene blue photoinactivation abolishes West Nile virus infectivity in vivo, Antiviral Res 68 (2005) 84–87. https://doi:10.1016/j.antiviral.2005.07.001.
[17] L. Costa, et al., Photodynamic inactivation of mammalian viruses and bacteriophages, Viruses 4 (2012) 1034–1074. https://doi:10.3390/v4071034.
[18] A.L.A. Monjo, et al., Photodynamic inactivation of Herpes simplex viruses, Viruses 10 (2018) 532. https://doi:0.3390/v10100532.
[19] N.S. Lebedeva, et al., The application of porphyrins and their analogues for inactivation of viruses, Molecules 25 (2020) 4368. https://doi:0.3390/molecules25194368.
[20] P.C.V. Conrado, et al., A systematic review of photodynamic therapy as an antiviral treatment: potential guidance for dealing with SARS-CoV-2, Photodiagnosis Photodyn. Ther. 34 (2021) 102221. https://doi:10.1016/j.pdpdt.2021.102221.
[21] M.R. Hamblin, Antimicrobial photodynamic therapy: new anti-infectives in the age of resistance, in: Photodynamic Medicine: from Bench to Clinic, 2016, pp. 549–571, https://doi.org/10.1039/9781782626824-00549. Chap. 29.
[22] G.S. Kulkarni, et al., A phase II clinical study of intravesical photo dynamic therapy in patients with BCG-unresponsive NMIBC (interim analysis), J. Clin. Oncol. 41 (2023) 528, https://doi.org/10.1200/JCO.2023.41.6_suppl.528.
[23] Y.J. Lei, et al., A study on ruthenium-based catalysts for pharmaceutical wastewater treatment, Water Sci. Technol. 64 (2011) 117–121. https://doi:0.2166/wst.2011.585.
[24] S. Monro, et al., Transition metal complexes and photodynamic therapy from a tumor-centered approach: challenges, opportunities, and highlights from the development of TLD1433, Chem. Rev. 119 (2019) 797–828, https://doi.org/10.1021/acs.chemrev.8b00211.
[25] F. Lambert, et al., Titration of human coronaviruses, HCoV-229E and HCoV-OC43, by an indirect immunoperoxidase assay, Methods Mol. Biol. 454 (2008) 93–102. https://doi:10.1007/978-1-59745-181-9_8.
[26] P. Kaspler, et al., A ruthenium(II) based photosensitizer and transferrin complexes enhance photo-physical properties, cell uptake, and photodynamic therapy safety and efficacy, Photochem. Photobiol. Sci. 15 (2016) 481–495. https://doi:10.1039/c5pp00450k.
[27] D. Korneev, et al., Ultrastructural aspects of photodynamic inactivation of highly pathogenic avian H5N8 influenza virus, Viruses 11 (2019) 955. https://doi:10.3390/v11100955.
[28] A.Z. Pevec, et al., As(2)O(3) oxidation by vitamin C: cell culture studies, Biometals 25 (2012) 103–113. https://doi:0.1007/s10534-011-9486-6.
[29] R. Khaengraeng, R.H. Reed, Oxygen and photoinactivation of Escherichia coli in UVA and sunlight, J. Appl. Microbiol. 99 (2005) 39–50. https://doi:10.1111/j.1365-2672.2005.02606.x.
[30] T.W. Chang, R.C. Heel, Ribavirin and inosiplex: a review of their present status in viral diseases, Drugs 22 (1981) 111–128. https://doi:0.2165/00003495-198122020-00002.
[31] E. De Clercq, Antiviral agents: characteristic activity spectrum depending on the molecular target with which they interact, Adv. Virus Res. 42 (1993) 1–55. https://doi:10.1016/s0065-3527(08)60082-2.
[32] Jr.H.C. Bodenheimer, et al., Tolerance and efficacy of oral ribavirin treatment of chronic hepatitis C: a multicenter trial, Hepatology 26 (1997) 473–477. https://doi:10.1002/hep.510260231.
[33] S.S. Jean, P.I. Lee, P.R. Hsueh, Treatment options for COVID-19: the reality and challenges, J. Microbiol. Immunol. Infect. 53 (2020) 436–443. https://doi:10.1016/j.jmii.2020.03.034.
[34] R.H. Williams, et al., Mycophenolic acid: antiviral and antitumor properties, J. Antibiot.(Tokyo). 21 (1968) 463–464. https://doi:10.7164/antibiotics.21.463.
[35] J. Neyts, E. De Clercq, Mycophenolate mofetil strongly potentiates the anti-herpesvirus activity of acyclovir, Antiviral Res 40 (1998) 53–56. https://doi:10.1016/s0166-3542(98)00047-3.
[36] L.L. Hermann, K.M. Coombs, Inhibition of reovirus by mycophenolic acid is associated with the M1 genome segment, J. Virol. 78 (2004) 6171–6179. https://doi:10.1128/JVI.78.12.6171-6179.2004.
[37] J. Marotti, et al., Photodynamic therapy can be effective as a treatment for herpes simplex labialis. Photomed, Laser Surg 27 (2009) 357–363. https://doi:10.1089/pho.2008.2268.
[38] M.A. Munegowda, et al., Efficacy of ruthenium coordination complex-based Rutherrin in a preclinical rat glioblastoma model, Neurooncol. Adv 1 (2019) vdz006. https://doi:10.1093/noajnl/vdz006.
[39] J.A. Willis, et al., Photodynamic viral inactivation: recent advances and potential applications, Appl. Phys. Rev. 8 (2021) 021315. https://doi:10.1063/5.0044713.
[40] G. Shi, et al., Ru(II) dyads derived from alpha-oligothiophenes: a new class of potent and versatile photosensitizers for PDT, Coord. Chem. Rev. 282 (2015) 127–138, https://doi.org/10.1016/j.ccr.2014.04.012.
[41] P.F. Wright, R.G. Webster, in: Fields Virology, D. Knipe, et al. (Eds.), Orthomyxoviruses, Lippincott Williams & Wilkins, Philadelphia, 2001, pp. 1533–1579.
[42] F. Krammer, et al., Influenza, Nat. Rev. Dis. Prim. 4 (2018) 3, https://doi.org/10.1038/s41572-018-0002-y.
[43] M.M.C. Lai, S. Perlman, L.J. Anderson, in: Fields Virology, D. Knipe, P.M. Howley (Eds.), Coronaviridae, Lippincott WIlliams & Wilkins, Philadelphia, 2007, pp. 1305–1335.
[44] A.H. de Wilde, et al., Host factors in coronavirus replication. Curr, Topics Microbiol. Immunol. 419 (2018) 1–42. https://doi:10.1007/82_2017_25.
[45] B.D. Lindenbach, et al., in: Fields Virology, D.M. Knipe, P.M. Howley (Eds.), Flaviviridae: the Viruses and Their Replication, Lippincott Williams & Wilkins, Philadelphia, 2013, pp. 712–746.
[46] K. van den Elsen, J.P. Quek, D.H. Luo, Molecular insights into the flavivirus replication complex, Viruses 13 (2021) 956. https://doi:10.3390/v13060956.
[47] B. Roizman, D. Knipe, R.J. Whitley, in: Fields Virology, D. Knipe, P.M. Howley (Eds.), Herpes Simplex Viruses, Lippincott Williams & WIlkins, Philadelphia, 2007, pp. 2501–2601.
[48] E.B. Draganova, M.K. Thorsen, E.E. Heldwein, Nuclear egress, Curr. Issues Mol. Biol. 41 (2021) 125–170. https://doi:10.21775/cimb.041.125.
[49] B. Moss, in: Fields Virology, D. Knipe, P.M. Howley (Eds.), Poxviruses, Lippincott Williams & Wilkins, Philadelphia, 2007, pp. 2905–2945.
[50] X.Z. Meng, et al., Vaccinia virus A6 is a two-domain protein requiring a cognate N-terminal domain for full viral membrane assembly activity, J. Virol. 91 (2017) e02405, 16, https://doi:10.1128/JVI.02405-16.

[51] A. Ono, Viruses and lipids, Viruses 2 (2010) 1236–1238. https://doi:10.3390/v2051236.
[52] N. Watabe, et al., Oxidation decomposition of unsaturated fatty acids by singlet oxygen in phospholipid bilayer membranes, J. Oleo Sci. 56 (2007) 73–80. https://doi:10.5650/jos.56.73.
[53] A. Ayala, M.F. Muñoz, S. Argüelles, Lipid peroxidation: production, metabolism, and signaling mechanisms of malondialdehyde and 4-hydroxy-2-nonenal, Oxid. Med. Cell. Longev. 2014 (2014) 360438. https://doi:10.1155/2014/360438.